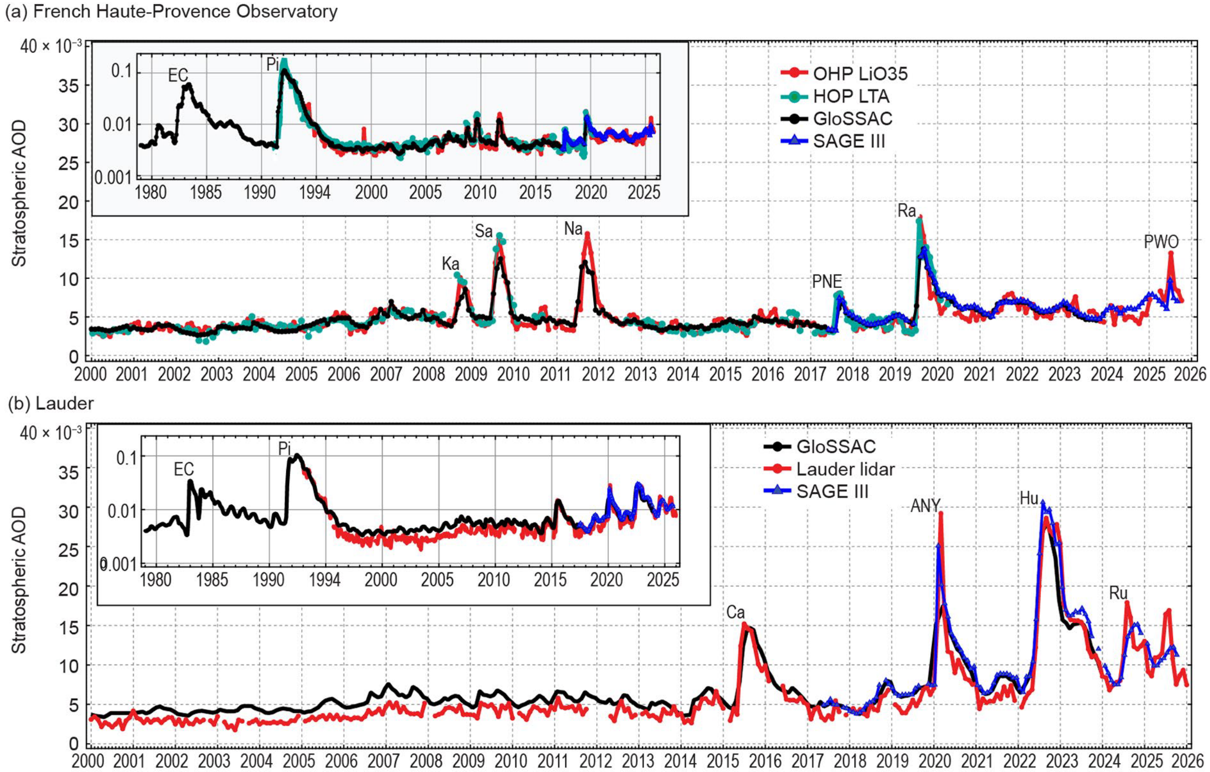

Fig. 2.72. Time series of monthly mean aerosol optical depth at 532 nm of the stratospheric overworld (380 K; 33 km) from ground-based lidars at (a) French Observatoire de Haute Provence (OHP, 43.9°N, 5.7°E, Stratospheric Ozone Lidar [LiO3S] and the Lidar Temperature Aerosol [LTA] instruments) and (b) New Zealand's Lauder station (45°S, 179°E, Lauder aerosol lidar) and the corresponding monthly/zonal-mean values from satellite observations within 40°N–50°N and 50°S–40°S latitude bands from ISS's Stratospheric Aerosol and Gas Experiment III (SAGE III) instrument and Global Space-based Stratospheric Aerosol Climatology (GloSSAC) merged satellite record. The embedded panels display the log-scaled time series from the beginning of the GloSSAC record. The literal notations indicate the most significant volcanic eruptions: El Chichon (EC), Pinatubo (Pi), Kasatochi (Ka), Sarychev (Sa), Nabro (Na), Raikoke (Ra), Calbuco (Ca), Hunga (Hu), and Ruang (Ru); and wildfire events: Pacific Northwest Event (PNE) in British Columbia, Canada and Australian New Year (ANY) super outbreak; Panboreal Wildfire Outbreak (PWO).

6. STRATOSPHERIC OZONE

—W. Steinbrecht, M. Weber, C. Arosio, R. van der A, L. M. Ciasto, M. Coldewey-Egbers, S. Davis, D. Degenstein, P. Effertz, V. E. Fioletov, L. Flynn, S. M. Frith, L. Froidevaux, S. Godin-Beekmann, J. de Laat, T. Leblanc, D. Loyola, E. Maillard Barras, I. Petropavlovskikh, R. Querel, A. Rozanov, M. L. Santee, V. Sofieva, K. Tourpali, R. Wang, T. Warnock, and J. D. Wild

Almost all ozone in the atmosphere, about 90% of the total column, resides in the stratosphere. On timescales shorter than a year, transport processes in the lower stratosphere are the most important source of total column ozone variations (e.g., Chipperfield et al. 2018). Chemical ozone loss due to anthropogenic ozone-depleting substances is important for springtime polar "ozone holes" and for decadal ozone changes (WMO 2022). The international Montreal Protocol has successfully banned production and consumption of ozone-depleting substances. Their atmospheric concentrations have been declining slowly since about 2000, but year-to-year variations of ozone are relatively unaffected. Full recovery of the ozone layer is not expected for another few decades (WMO 2022).

For the year 2025, Plate 2.1ah shows that total column ozone values over much of the North Hemisphere (NH) were up to 30 Dobson Units (DU) below the 1998–2008 average. This was due to weak planetary wave activity in the NH 2024/25 winter stratosphere (e.g., https://ozonewatch.gsfc.nasa.gov/meteorology/NH.html), resulting in weak poleward transport of ozone in the NH and a strong Arctic winter vortex in January and February, with significant chemical ozone depletion and very low total column ozone in February and March over Eurasia. This low ozone signature from January to March remained in the annual mean anomaly shown in Plate 2.1ah.

While total column ozone over the NH mid- and high latitudes changed from above normal in 2024 (Newman et al. 2024) to below normal in 2025, total column ozone over the

SH mid- and high latitudes was above normal in both 2024 and 2025, by up to 60 DU in 2025 (Plate 2.1ah). The low values near 60°S, 45°W were due to an unusual shift of the remainder of the Antarctic ozone hole towards South America in November and December 2025 (e.g., https://woudc.org/en/data/products/ozone-maps/archive). Overall, planetary wave activity and poleward ozone transport in the SH were above normal in 2025 (and in 2024), and the 2025 and 2024 Antarctic ozone holes were less pronounced than in previous years (see section 6h for details).

Between 30°S and 30°N, total column ozone in 2025 was affected by the easterly shear phase of the quasi-biennial oscillation of equatorial winds (QBO) and by a weak La Niña (cool phase; section 2e3). The situation was almost the opposite of 2024, which had a westerly shear QBO phase and an El Niño (warm phase) in the first months of the year. The QBO-induced residual circulation (Baldwin et al. 2001) resulted in reduced (up to 2 DU below normal) total column ozone over the equator in 2025 and enhanced (by up to 10 DU) values around 20°N and 20°S. These alternating bands of high and low total ozone are visible in Plate 2.1ah. La Niña, with cooler sea surface temperatures in the equatorial Pacific, weakly counteracted the QBO-induced anomalies (Oman et al. 2013; Domeisen et al. 2019), as seen in slightly higher total ozone columns above the equatorial Pacific and slightly lower columns above Indonesia and Australia (Plate 2.1ah).

The long-term evolution of total column ozone is plotted in Fig. 2.73. The data clearly show the depletion of ozone from the 1970s to the mid-1990s, caused by increasing concentrations of anthropogenic ozone-depleting substances, and the beginning of a slow recovery since about 2000 (WMO 2022). Compared to 2024 and other recent years, the 2025 total column ozone values were similar for four of the six latitude bands (near-global 60°S–60°N, tropical 20°S–20°N, Southern Hemisphere (SH) 35°S–60°S, and the SH polar 60°S–90°S). For the NH midlatitude and polar bands, total column ozone in 2025 was much lower than that in 2024 (as explained above) and slightly higher compared to 2021 to 2023.

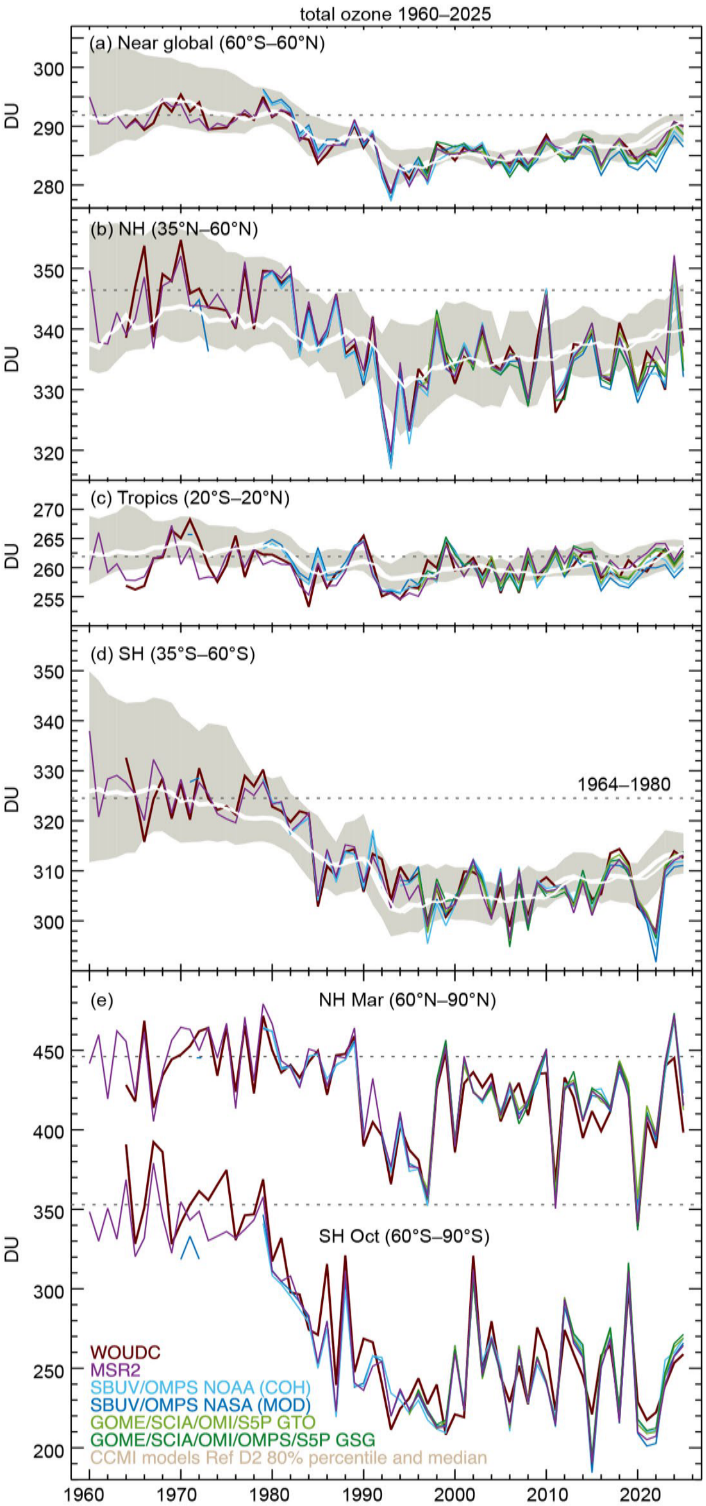

Fig. 2.73. Time series of annual mean total column ozone (DU) in four zonal bands: (a) near global (60°S–60°N), (b) Northern Hemisphere (35°N–60°N), (c) tropics (20°S–20°N), and (d) Southern Hemisphere (35°S–60°S). Panel (e), time series of polar total column ozone (60°S–90°S; DU) for the Northern Hemisphere (NH) and the Southern Hemisphere (SH) in Mar and Oct, respectively, the months when polar ozone losses are largest. The dotted gray lines in each panel show the average for 1964–1980, calculated from the World Ozone and Ultraviolet Radiation Data Centre's (WOUDC) data. The observational data for 2025 are preliminary. The thick white lines and gray shading in (a)–(d) show the median and 80th percentile range from model simulations by the Chemistry-Climate Model Initiative CCMI-2022 (refD2 simulations; Abalos et al. 2026). All datasets are shifted to the same average value over the reference period 1998–2008 as the multi-instrument mean.

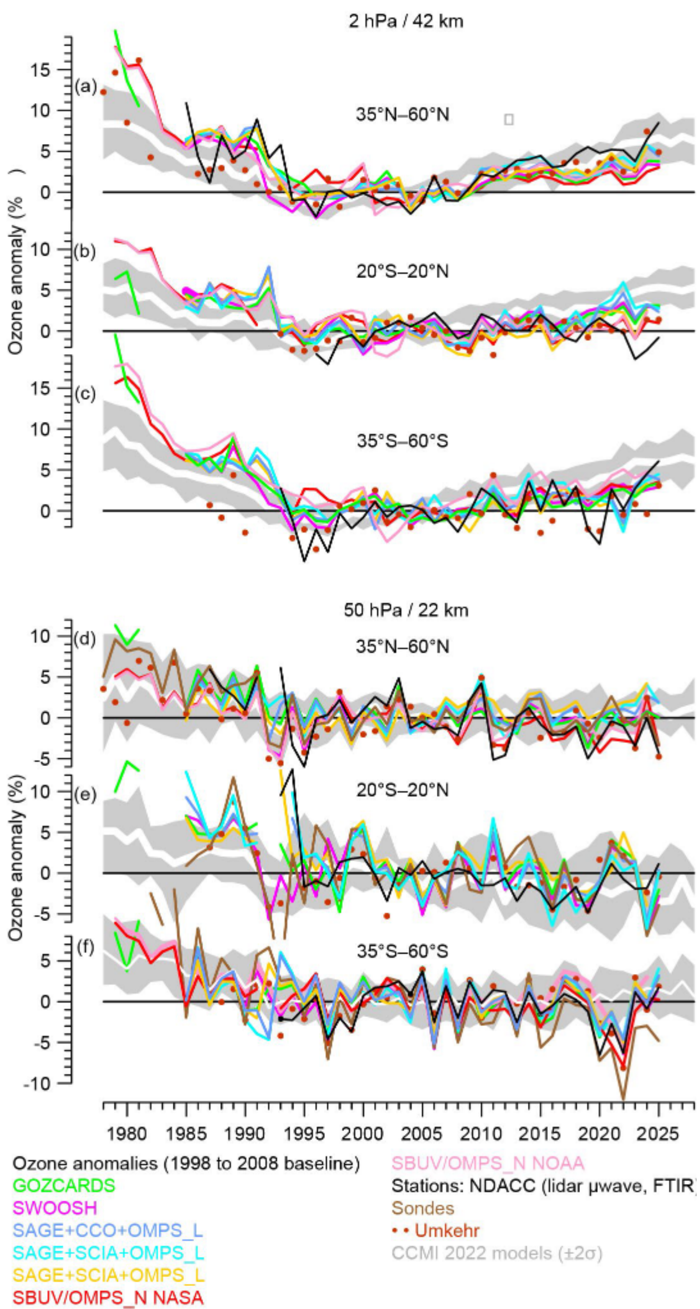

Using ozone profile data, Fig. 2.74 shows the long-term behavior of ozone at two levels in the stratosphere (Steinbrecht et al. 2017; WMO 2022). At the 2-hPa level in the upper stratosphere (about 42-km altitude), chlorine from anthropogenic ozone-depleting substances and atmospheric temperature have the largest influence, while the transport processes that also influence total column ozone are most important at the 50-hPa level in the lower stratosphere (about 22 km).

Consistent with total column ozone in Fig. 2.73, lower stratospheric ozone anomalies in 2025 in Figs. 2.74d–f show values similar to those in recent years, higher than in 2024 in the tropical 20°S–20°N band and in the SH 35°S–60°S band, and lower than in 2024 in the NH 35°N–60°N band. For all three bands, the observed long-term evolution is generally consistent with the range of ozone values (gray) simulated by the CCMI-2022 modeling experiments (Abalos et al. 2026), although the observed data in the NH (Fig. 2.74d) are often lower in recent years. The observed low values from 2020 to 2023 in the SH (Fig. 2.74f) were due to extreme events not accounted for in the model simulations—among them the Australian New Year wildfires in 2020 and the Hunga Tonga volcanic eruption in 2022.

In the upper stratosphere, 2025 ozone anomalies in Figs. 2.74a–c are comparable to or higher than anomalies in the last couple of years. The sparse station data (e.g., NDACC, black lines) do not always agree with the zonal mean data from the satellites. Compared to the CCMI-2022 model simulations (gray), the observed anomalies in recent years lie at the lower end of the simulated range. These simulations account for the expected evolution of

Fig. 2.74. Annual mean anomalies of ozone (%) in the (a)–(c) upper stratosphere near 42-km altitude or 2-hPa pressure, and in the (d)–(f) lower stratosphere near 22 km or 50 hPa for three zonal bands: (a),(d) 35°N–60°N, (b),(e) 20°S–20°N (tropics), and (c),(f) 35°S–60°S, respectively. Anomalies are referenced to the 1998–2008 baseline. Annual means are plotted at the tick marks of the start of each year. Colored lines are long-term records obtained by merging different limb (Global Ozone Chemistry and Related Trace Gas Data Records for the Stratosphere [GOZCARDS], Stratospheric Water and Ozone Satellite Homogenized [SWOOSH], Stratospheric Aerosol and Gas Experiment [SAGE]+Climate Change Initiative [CCI]+Ozone Mapping and Profiler Suite Limb Profiler [OMPS-LP], SAGE+Scanning Imaging Absorption Spectrometer for Atmospheric Chartography [SCIAMACHY]+OMPS-LP, SAGE+Optical Spectrograph and InfraRed Imaging System [OSIRIS]+OMPS-LP) and nadir-viewing (Solar Backscatter Ultraviolet Radiometer [SBUV], OMPS Nadir Profile [OMPS-NP]) satellite instruments. The nadir-viewing instruments have a much coarser altitude resolution than the limb-viewing instruments. This can cause differences in some years, especially at 50 hPa. Red dots are results from ground-based Umkehr data (Petropavlovskikh et al. 2025). The black line is from merging ground-based ozone records at seven Network for the Detection of Atmospheric Composition Change (NDACC) stations employing differential absorption lidars and microwave radiometers. See Steinbrecht et al. (2017), WMO (2022), and Arosio et al. (2019) for details on the various datasets. The gray shaded areas show the range of chemistry-climate model simulations from the Chemistry-Climate Model Initiative (CCMI-2022, refD2 simulations; Abalos et al. 2026), with the white line showing the multi-model median. Ozone data for 2025 are still preliminary.

chlorine (and bromine) from anthropogenic ozone-depleting substances and for stratospheric cooling due to increasing greenhouse gas concentrations; however, stratospheric chlorine abundances might be underestimated (Lickley et al. 2024).

Overall, stratospheric ozone in 2025 was comparable to values seen in recent years, and consistent with understanding and expectations summarized in WMO (2022).

7. STRATOSPHERIC WATER VAPOR

—S. M. Davis, E. A. Asher, H. Vömel, R. M. Stauffer, E. G. Hall, and K. H. Rosenlof

In 2025, tropical lowermost stratospheric water vapor (WV) concentrations returned to anomalously high values following a year (2024) in which the values were relatively low. The lingering effects of the January 2022 eruption of the Hunga volcano (Millán et al. 2022; Vömel et al. 2022) were evident in other regions of the stratosphere. Deseasonalized tropical lower-stratospheric WV anomalies (using a climatological base period of 2004–21 to exclude the effects of the large Hunga perturbation) of air entering the stratosphere (near the tropopause at 82 hPa) were positive for all but the final months of the year (Figs. 2.75a,c, 2.76, 2.77), consistent with the anomalously positive values observed in the last five years.

Although the cause of the recent positive "trend" remains an active area of research, there are potential contributions from surface warming, volcanoes (including moderate eruptions in addition to Hunga), wildfires, and natural interannual to decadal-scale variability (Konopka et al. 2022; Peng et al. submitted; Tao et al. 2023; Zolghadrshojaee et al. 2024).

Zonal-mean WV calculated from satellite measurements shows that lingering positive anomalies from Hunga were evident in 2025 in the tropical upper stratosphere (above 10 hPa, Figs. 2.75a, 2.76) and middle stratosphere (particularly the SH; Figs. 2.75b, 2.76), with some of these WV anomalies being most positive in the extratropics and high latitudes (see hatched regions, Fig. 2.76). Positive WV anomalies, including many record-high values, were also present in the lower stratosphere throughout most of 2025 (Fig. 2.76). These lower stratospheric record-high anomalies were most geographically coherent from May through the end of the year, spanning from nearly pole to pole a few kilometers above the tropopause, and ascending over this time in the tropics in a manner that appears consistent with the yearly progression of the so-called "tropical tape recorder" (Mote et al. 1996).

Attribution of these lower-stratosphere anomalies is subject to ongoing research, but they are plausibly explained as some combination of Hunga-impacted air and anomalously moist air entering the stratosphere in the tropics. The tropical WV anomalies are expected to be primarily caused by anomalies in tropical tropopause temperatures, which affect freeze-drying of air ascending into the stratosphere. Indeed, lower-stratospheric

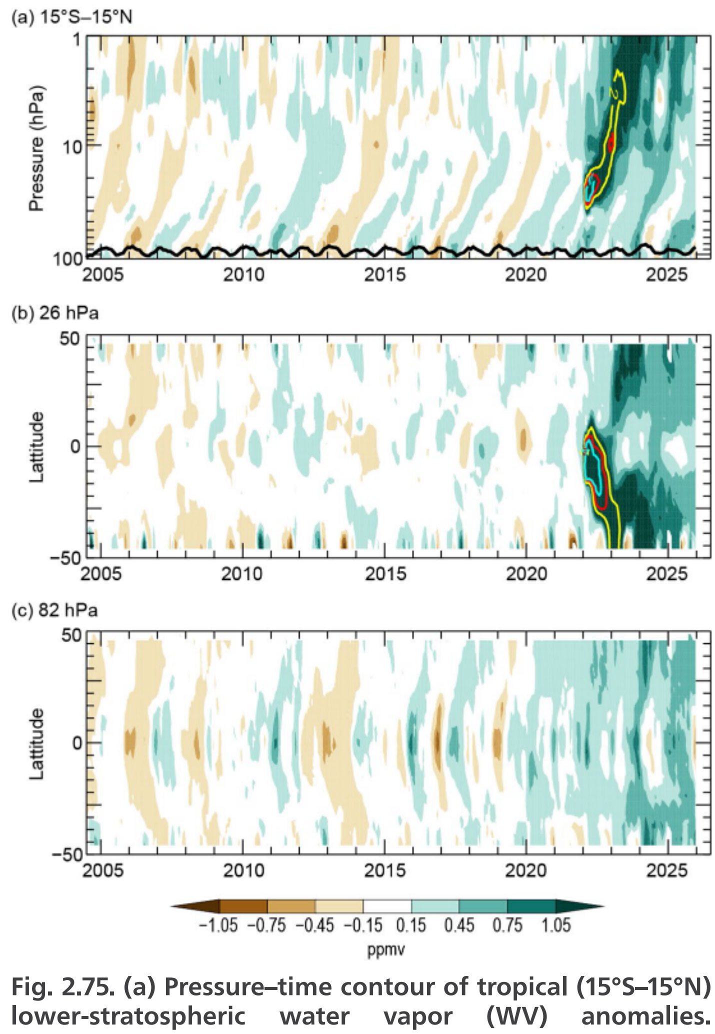

Fig. 2.75. (a) Pressure–time contour of tropical (15°S–15°N) lower-stratospheric water vapor (WV) anomalies. (b),(c) Latitude–time contour of WV anomalies at (b) 26 hPa (middle stratosphere) and (c) 82 hPa (lower stratosphere). Yellow, red, and cyan contour lines represent values of +2, +3, and +4 ppmv, respectively (no values in [c] exceed +2 ppmv). The black line in (a) shows the MERRA-2 tropical cold point pressure. All panels are based on merged satellite data from the Stratospheric Water and Ozone Satellite Homogenized version 2.72 (SWOOSH v2.72). Anomalies are differences from the mean 2004–21 water vapor mixing ratios (ppmv) for each month. Tick marks denote the beginning of each year.